Coherent control of high-order-harmonic generation via tunable plasmonic bichromatic near fields in a metal nanoparticle

Wen-Xing Yang,[1,2,*] Xiao-Tao Xie,[3] Ai-Xi Chen,[4] Ziwen Huang,[1] and Ray-Kuang Lee[2,5]
[1]*Department of Physics, Southeast University, Nanjing 210096, China*
[2]*Institute of Photonics Technologies, National Tsing-Hua University, Hsinchu 300, Taiwan*
[3]*School of Physics and Information Technology, Shanxi Normal University, Xi'an 710062, China*
[4]*Department of Applied Physics, East China Jiaotong University, Nanchang 330013, China*
[5]*Physics Division, National Center for Theoretical Science, Hsinchu 300, Taiwan*
(Received 10 December 2015; published 4 May 2016)

We present a theoretical investigation of high-order-harmonic generation (HHG) via bichromatic plasmonic near fields with metal nanoparticles. Bichromatic plasmonic near fields, which depend on temporal waveform synthesis, are generated when a metallic nanoparticle subjected to a moderate-intensity ($<10^{12}$ W/cm^2) bichromatic few-cycle pulse. By means of a windowed Fourier transform of the time-dependent acceleration, we show that the differences in energies and level crossing between the adiabatic states of a two-level Hamiltonian are responsible for the cutoff energy of harmonics. Thus, we can manipulate the adiabatic states, and consequently the HHG spectra, by means of the bichromatic plasmonic near fields. In contrast to the case of a monochromatic field alone, a significant cutoff extension can be achieved via optimization of the bichromatic few-cycle pulse. Moreover, the supercontinuum in the bichromatic field shows a higher energy spectrum along with a broader bandwidth, which is beneficial for the efficient generation of broadband-isolated ultrashort extreme ultraviolet pulses from few-cycle laser fields.

DOI: 10.1103/PhysRevA.93.053806

I. INTRODUCTION

High-order-harmonic generation (HHG) is a well-established process for producing extreme-ultraviolet (XUV) pulses and attosecond pulses, which also acts as a prerequisite for the attophysics [1–12]. This physical process can be well understood by the three-step model [4–6]: ionization, acceleration, and recombination of the electrons, where bound-continuum transitions driven by an intense laser field ($\sim 10^{14}$ W/cm^2) are involved. In a necessary intensity regime (10^{12}–10^{14} W/cm^2) [13–21], apart from the three-step model [4–6], a simplified model has been proposed to describe HHG [15–19]. In this regime where bound-bound transition only is considered, HHG can be described in a completely different model called the "two-level atom" [15–19]. In this theory [16], HHG is a consequence of the population transfer between the field-dependent states that come from diagonalization of the two-level Hamiltonian.

HHG requires peak intensities higher than 10^{14} W/cm^2 for the incident field, thus, HHG typically relies on complex and expensive femtosecond laser amplifier systems with repetition rates in the few-kilohertz range. Over the past decades, different approaches have been followed to achieve HHG with a significant reduction in the threshold pump power. One of the effective schemes was obtained from surface plasmonic resonances that can locally amplify laser field using gold bow-tie-shaped nanostructures [22]. Therein, when a low-intensity femtosecond pulse drives the plasmonic mode in a metallic nanoparticle (MNP), a highly amplified electric field can be created, and with injection of noble atomic gases near the MNP, HHG can be achieved. Recently, there have been numerous studies [22–44] on HHG driven by enhanced fields using plasmons, in which some novel prospects for and interpretation of the electron dynamics induced by these enhanced fields from dielectric nanoparticles, MNPs, and metal nanotips are presented.

It is noteworthy that, by using the two-level atom model [15–19], we have investigated HHG in an MNP–semiconductor quantum dot (SQD) hybrid system with a moderate-intensity monochromatic field [43]. Therein, the energies and populations between the adiabatic states of the two-level Hamiltonian, and consequently the HHG spectra, can be manipulated by modulating the interparticle distance between the MNP and the SQD. However, it is difficult to manipulate the few-nanometer distance between MNP and SQD in technology. Thus, another question arises: Can we control HHG with a more effective approach than the previous scheme [43]? In this paper, we investigate HHG using bichromatic few-cycle plasmonic near fields in an SQD and MNP hybrid system. This should not be confused with the investigation of HHG using enhanced near fields that drive the bound to the continuum transition in the surrounding atomic or molecular gas [22–42]. We show that high-order harmonics can be produced even at the modest intensity of the few-cycle pulse where both tunneling and multiphoton ionizations hardly take place. It is found that the differences in energies between the adiabatic states of the two-level Hamiltonian are responsible for the cutoff energy of harmonics. Thus we can manipulate the adiabatic states, and consequently the HHG process, by modulating the relative intensity and the relative phase of the bichromatic fields. In contrast to the case of a monochromatic field alone [43], a significant cutoff extension can be achieved via optimization of the bichromatic few-cycle pulse and the supercontinuum in the bichromatic field shows a higher energy and a broader bandwidth, which is beneficial for the efficient generation of broadband-isolated ultrashort XUV pulses from few-cycle laser fields.

*wenxingyang2@126.com

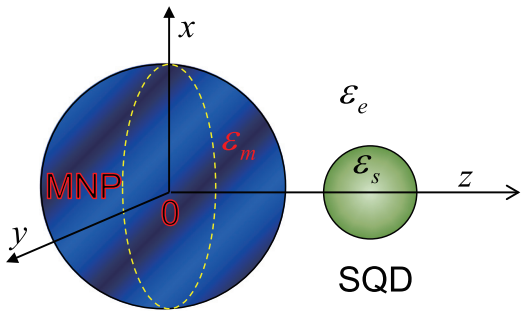

FIG. 1. Schematic of the hybrid system consisting of an SQD and an MNP. The centers of the two particles are separated by a distance represented by R. The incident bichromatic few-cycle pulse propagates along the y axis with polarization along the z axis.

II. THE MODEL AND BASIC EQUATIONS

The hybrid system under consideration is illustrated in Fig. 1. The device is composed of a spherical MNP of radius a and a spherical SQD of radius b in an environment with dielectric constant ϵ_0. The center-to-center distance between the two particles is denoted R. The parameters of the system, i.e., the size of the SQD and MNP and the center-to-center distance between two particles, are chosen such that the SQD has small dimensions, $b \ll a$, and the size of the MNP is constrained as $a < R$. We consider this hybrid system driven by a bichromatic few-cycle pulse. In our simulation, the bichromatic few-cycle pulse is synthesized by a fundamental pulse and a control pulse. The incident bichromatic few-cycle pulse can be synthesized by a fundamental pulse and an additional low-frequency control pulse with electric field

$$E(t) = E_0 f(t)\sin[\omega_0(t-2T_0)] + qE_0 f(t)\sin\left[\tfrac{1}{2}\omega_0(t-2T_0)+\phi\right], \quad (1)$$

where E_0 and ω_0 are the electric-field amplitude and the angular frequency ($T_0 = 2\pi/\omega_0$ is the optical oscillation cycle time) of the fundamental driving pulse. The parameters q and ϕ denote the field-strength ratio and relative phase between the fundamental and the control pulses, respectively. The pulse envelope is centered at $2T_0$ and is given by $f(t) = \exp[-4\ln 2(\frac{t-2T_0}{\tau})^2]$, with τ the pulse duration (full width at half-maximum). In our simulation, the incident bichromatic pulse propagates along the y axis with polarization along the z axis.

We focus on the response of a hybrid nanostructure consisting of an SQD and an MNP subjected to an applied bichromatic few-cycle pulse in a weak-field regime where both tunneling and multiphoton ionization hardly take place. Here the SQD is characterized by a two-level system, with $|0\rangle$ being the ground state and $|1\rangle$ being the single-exciton state. The electric field excites both the interband transition in the SQD and the surface plasmon in the MNP. This surface plasmon influences the exciton and induces electromagnetic interactions between exciton and plasmon [45–47]. This interaction is responsible for the coupling between the two particles and leads to the Förster energy transfer [48]. The total field felt by the SQD can be given as $E_{\rm SQD}(t) = E(t) + gP_M/(\epsilon_{\rm eff}R^3)$, where $\epsilon_{\rm eff} = (2\epsilon_0+\epsilon_s)/3\epsilon_0$, with ϵ_0 and ϵ_s the dielectric constants of the background medium and the SQD, respectively. When $E(t)$ is parallel to the long axis of the MNP, the constant g is 2 for the complex with a to-the-end orientation. The dipole of the MNP $P_M = \alpha_M E_M$ comes from the charge induced on the surface of the MNP with the dipole polarization $\alpha_M = \epsilon_0(\epsilon_m-\varepsilon_0)/3[(\epsilon_m-\epsilon_0)+\epsilon_0]$ and the field felt by the MNP $E_M(t) = E(t) + gP_{\rm SQD}/(\epsilon_{\rm eff}R^3)$. The corresponding enhancement factor within the hybrid complex is $f(\omega) = 1 + g\alpha_M/(\epsilon_{\rm eff}R^3)$. The dipole of the SQD is $P_{\rm SQD} = \mu[C_0^*(t)C_1(t) + C_1^*(t)C_0(t)]$, where μ is the dipole moment of the transition $|0\rangle \leftrightarrow |1\rangle$ and $C_j(t)$ ($j = 0,1$) is the probability amplitude of state $|j\rangle$.

An SQD with exciton vacuum state $|0\rangle$ and exciton state $|1\rangle$ can be described by a two-level atom model in which the SQD interacts with a classical bichromatic driving field, and the Hamiltonian in field-free states can be given by

$$\frac{H^D}{\hbar} = \begin{pmatrix} -\frac{1}{2}\omega_{10} & \Omega(t) \\ \Omega(t) & \frac{1}{2}\omega_{10} \end{pmatrix}, \quad (2)$$

where ω_{10} and $\Omega(t) = \mu E(t) f(\omega)/\hbar$ are the transition frequency between state $|0\rangle$ and state $|1\rangle$ and the time-dependent Rabi frequency of the plasmonic near field, respectively. Within this picture, we define the time-dependent wave function $\psi(t) = C_0(t)|0\rangle + C_1(t)|1\rangle$. The evolution of the system can be described by the time-dependent Schrödinger equation $i\hbar d\psi(t)/dt = H^D\psi(t)$. In order to diagonalize the field-free Hamiltonian H^D, we adopt an important set of bases called adiabatic bases, which means that the states follow the field. The diagonal Hamiltonian is obtained by the unitary transformation $H^A(t) = UH^DU^\dagger$ with $U = \exp[-i\theta\sigma_y]$, where $\theta = \frac{1}{2}\arctan(2\Omega(t)/\omega_{10})$ and σ_y is the Pauli matrix. Applying this transformation, the adiabatic states $|0\rangle^A$ and $|1\rangle^A$ can be given by $|0\rangle^A = \cos\theta|0\rangle + \sin\theta|1\rangle$ and $|1\rangle^A = -\sin\theta|0\rangle + \cos\theta|1\rangle$, respectively. In the adiabatic basis, the adiabatic energies of the two adiabatic states can be calculated as $\epsilon_\pm = \pm\frac{1}{2}\sqrt{\omega_{10}^2 + 4\Omega^2(t)}$. Then $\psi(t)$ can be written under the adiabatic basis $\psi(t) = d_0(t)|0\rangle^A + d_1(t)|1\rangle^A$, with the corresponding motion equation

$$i\frac{\partial}{\partial t}\begin{pmatrix} d_0(t) \\ d_1(t) \end{pmatrix} = \begin{bmatrix} -\frac{1}{2}\Omega^A(t) & \frac{-i\omega_{10}\dot{\Omega}(t)}{[\Omega^A(t)]^2} \\ \frac{i\omega_{10}\dot{\Omega}(t)}{[\Omega^A(t)]^2} & \frac{1}{2}\Omega^A(t) \end{bmatrix}\begin{pmatrix} d_0(t) \\ d_1(t), \end{pmatrix} \quad (3)$$

with $\Omega^A(t) = \varepsilon_+ - \varepsilon_-$ as the energy difference between the two adiabatic states. The harmonic spectrum can be obtained by Fourier transforming the time-dependent dipole acceleration, which is given by

$$P(\omega) = \left|\int a(t)e^{-i\omega t}dt\right|^2, \quad (4)$$

where $a(t) = -\mu\omega_{10}^2[A(t)\cos 2\theta + B(t)\sin 2\theta] + 2\omega_{10}\mu\Omega(t)[B(t)\cos 2\theta - A(t)\sin 2\theta]$ is the time-dependent dipole acceleration with $A(t) = d_0^*(t)d_1(t) + d_1^*(t)d_0(t)$ and $B(t) = |d_0(t)|^2 - |d_1(t)|^2$. The dipole acceleration $a(t)$ is the superposition of two terms, i.e., the crossed term $A(t)$ and the population difference $B(t)$ between the adiabatic states $|0\rangle^A$ and $|1\rangle^A$. It has been confirmed that HHG is always related to abrupt population transfers [16], which leads to periodic level crossings and avoided level crossings

at particular times. Without any loss of generality, we define that t_1 and t_2 correspond to the level-crossing times and the avoided level-crossing times, respectively. In order to extract these times from the time-dependent dipole, we can examine the detailed spectrum and temporal structure of HHG via a time-frequency analysis [49,50] of HHG by utilizing the wavelet transform of the induced dipole acceleration $a(t)$, which is given by

$$S_\omega(t,\omega) = \int a(t')\sqrt{\omega}W[\omega(t-t')]dt', \tag{5}$$

where $W(x)$ is a windowed oscillating function and is chosen to be the complex Morlet wavelet $W(x) = \frac{1}{\sqrt{\pi f_b}} e^{i2\pi f_c x} e^{-x^2/f_b}$, where f_c and f_b are dimensionless parameters, determining the wavelet center frequency and wavelet bandwidth, respectively.

In order to calculate the time-dependent dipole acceleration $a(t)$, we have to solve the motion equation, (3), in the adiabatic basis. As far as we know, no closed-form solution of the nonlinear differential equation, (3), exists for fields of arbitrary temporal profile in the present complex system. In the following, we employ the fourth-order Runge-Kutta algorithm approach for solving Eq. (3) numerically. In our simulation, the bichromatic few-cycle pulse is synthesized by a fundamental pulse and a control pulse. The frequency and peak intensity of the fundamental pulse are chosen as $\hbar\omega_0 = 0.25$ eV and $E_0 = 5.7 \times 10^{11}$ W/cm^2, respectively, with the duration $\tau = 1.5T_0$. The peak intensity of the control pulse is denoted qE_0. For the SQD, we take $\epsilon_s = 6\epsilon_0$ (with ϵ_0 the dielectric constant of the vacuum) and $\mu = 0.65e$ nm. For the exciton resonant energy we take $\hbar\omega_{10} = 2.5$ eV. These parameter values correspond to the typically CdSe-based quantum dots [51] and have been used in several previous works [47,52,53]. For the MNP, we take $\epsilon_m(\omega)$ as the bulk dielectric constant of gold as found experimentally [54]. For a small, spherical, gold MNP, we take the radius of the MNP $a = 7.5$ nm.

III. HIGH-ORDER-HARMONIC GENERATION

In this section, we focus on HHG resulting from the interaction of an SQD with localized surface plasmons. Plasmonic near fields are produced when an MNP is subject to a bichromatic few-cycle laser pulse. Here we consider a weak-field regime where both tunneling and multiphoton ionization hardly take place. The SQD is characterized by a two-level system, with $|0\rangle$ being the ground state and $|1\rangle$ the single-exciton state. Recently, we have shown that the particle diameters and interparticle distances can be optimized to support both a large field enhancement and a large interaction volume for HHG [43]. Differently from our previous work [43], here we consider the bichromatic driving field denoted by Eq. (1). Compared with Ref. [43], we find that the present work has the following merits: (i) instead of varying the distance between the MNP and the SQD, here the cutoff energy of harmonics can be extended by changing the field-strength ratio and relative phase between the fundamental and the control pulses; (ii) the connection between HHG and periodic level crossings is confirmed, i.e., the differences in energies between adiabatic states are responsible for the cutoff energy of harmonics; (iii) a high-energy and a broadbandwidth supercontinuum is achievable, which is beneficial for the efficient generation of broadband-isolated ultrashort XUV pulses from few-cycle laser fields; and (iv) a qualitative discussion of the plasmonic field enhancement of HHG in a realistic ordered array of gold nanoparticles is provided.

Depending on the temporal waveform synthesis of the bichromatic field, the cutoff of the spectra is given by the maximum of $\Omega^A(t)$. To obtain the maximum possible cutoff energy of HHG, the avoided level crossings between adiabatic states must occur at the time t_{2M} that the energy difference $\varepsilon_+ - \varepsilon_-$ reaches the maximum. Thus, to derive the level-crossing times t_1, as well as the time t_{2M} corresponding to the maximum cutoff energy, we should obtain the maximal value $\pm\varepsilon_M^A$ of the adiabatic energies $\varepsilon_\pm$. For the bichromatic field in Eq. (1), the explicit expression of the times t_1 and t_{2M} can be given by

$$\cos(\omega_0 t) + \frac{q}{2}\cos\left(\frac{1}{2}\omega_0 t + \phi\right) = 0, \tag{6}$$

$$\sin(\omega_0 t) + q\sin\left(\frac{1}{2}\omega_0 t + \phi\right) = 0. \tag{7}$$

The time corresponding to the maximum energy difference t_{2M} is defined by Eq. (6); the level crossing time t_1 is given by Eq. (7). From Eqs. (6) and (7), one finds that the times t_{2M} and t_1, as well as the corresponding maximal values, depend on the field-strength ratio q and the relative phase ϕ. Therefore, the time-dependent plasmonic enhanced field and adiabatic energies, as well as the harmonics spectra, can be controlled by the parameters q and ϕ. In the present paper, we provide comparative results for different cases, i.e., only the fundamental pulse $q = 0$, different relative phases ϕ, and different field-strength ratios q. First, we present the effects of the MNP on the incident bichromatic pulse. The corresponding plasmonic field enhancement spectra of the MNP for different field-strength ratios (i.e., $q = 0$, $q = 0.5$, and $q = 0.8$) and different relative phases (i.e., $\phi = 0$ and $\phi = \pi/2$) are shown in Fig. 2(a). This figure shows that modifying the incident pulse by the MNP has the direct consequence of enhancing and reshaping the field. Also, one finds from this figure that the enhancement effect for the bichromatic field case ($q \neq 0$) is more profound than that for only the fundamental field case ($q = 0$). The maximum field enhancement exceeds 7 for $q = 0.8$ and $\phi = 0$. In this case, the intensity of the incident pulse is enhanced up to intensities higher than 10^{12} W/cm^2, which is the necessary intensity to generate high-order harmonics. Compared with the results for $\phi = 0$, the figure also shows that the locations of enhanced temporal pulse peaks become small and deviate slightly with respect to time for the case of $\phi = \pi/2$. The corresponding harmonic spectra based on Eq. (4) for different field-strength ratios q and relative phases ϕ are shown in Fig. 2(b). One general common feature of the HHG power spectra for these different cases is the appearance of a plateau and a sharp cutoff. In comparison to the case of only a fundamental incident pulse ($q = 0$), the notable difference in the HHG power spectra is that the harmonics cutoff energy can be extended for the case of a bichromatic incident pulse ($q \neq 0$). As shown in Fig. 2(b), the cutoff energy is about $100\omega_0$ for $q = 0$, $230\omega_0$ for $q = 0.5$ and $\phi = 0$, $220\omega_0$ for $q = 0.5$ and $\phi = \pi/2$, $350\omega_0$ for $q = 0.8$

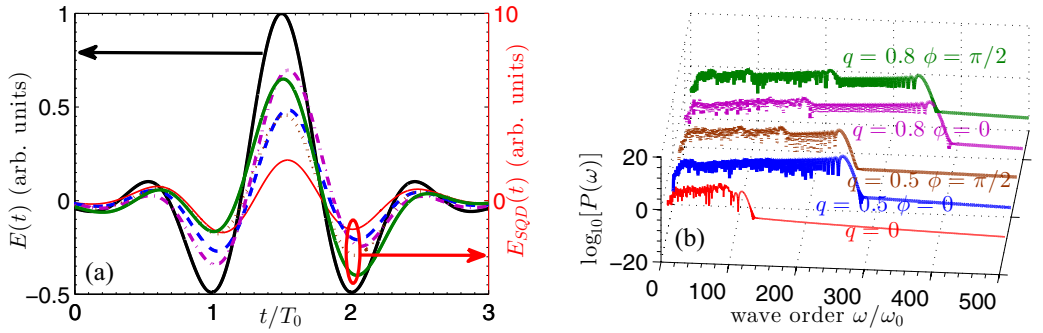

FIG. 2. (a) Field enhancement of an MNP on an incident Gaussian-shaped bichromatic pulse for different field-strength ratios q and relative phases ϕ, i.e., $q = 0$ (thin solid line); $q = 0.5$, $\phi = 0$ (dashed line); $q = 0.5$, $\phi = \pi/2$ (dotted line); $q = 0.8$, $\phi = 0$ (dash-dotted line); and $q = 0.8$, $\phi = \pi/2$ (thick solid line). (b) The corresponding HHG spectra for different cases. Other parameters are chosen as $a = 7.5$ nm, $R = 11$ nm, $\hbar\omega_0 = 0.25$ eV, and $\tau = 1.5T_0$.

and $\phi = 0$, and $320\omega_0$ for $q = 0.8$ and $\phi = \pi/2$, in which the maximal energy of the HHG can reach the XUV regime, i.e., 87.5 eV. These results imply that we can save the power of the incident field significantly for HHG with a high cutoff energy via choosing an appropriate additional control pulse. In addition, Fig. 2(b) also shows that the power spectrum of the HHG has an obvious dependence on the relative phase ϕ. One finds from this figure that the difference in the HHG power spectrum for different ϕ appears near the cutoff region, where a broadband quasicontinuum region can be observed for $\phi = 0$. Another difference in the HHG spectrum is that the maximal cutoff energy for $\phi = 0$ is higher than the one for $\phi = \pi/2$. As a matter of fact, the relative phase-dependent effects are more notable when the pulse becomes shorter [21,55].

Nevertheless, the power spectra of HHG alone do not provide enough information on the physical mechanism responsible for the cutoff extension. Concerning HHG, it has been shown that the periodic level crossings caused by the temporal dependence of the laser field are very important [16]. Therefore, in order to understand the harmonic spectra in this context, we should examine the interplay between these level crossings and HHG. In the following we perform simulation of the time evolution of field-dressed states by using the driven two-level atom model [15–17,43], which is very convenient for studying level crossings. Similarly to the classical three-step model, the driven two-level atom model can also be understood with three steps [16]: first, population transfers from the field-dressed state $|0\rangle^A$ to state $|1\rangle^A$ at level-crossing times t_1; second, the system's gaining energy from the field; and finally, population transfers from state $|1\rangle^A$ back to state $|0\rangle^A$ at the avoided level-crossing times t_2 accompanied by the energy released in the form of harmonic radiation. The main contribution to the highest harmonic generation takes place at time t_{2M}, corresponding to the maximal energy difference of the adiabatic states. The instantaneous frequency of harmonics is given by the energy difference between the two adiabatic states,

$$\Omega^A(t) = M\omega_p = \epsilon_+ - \epsilon_- = \sqrt{\omega_{10}^2 + 4\Omega^2(t)}. \tag{8}$$

The difference has a minimum of ω_{10} and a maximum of

$$\Omega^A_{\max}(t) = M_{\max}\omega_p = \sqrt{\omega_{10}^2 + 4\Omega^2_{\max}(t)}, \tag{9}$$

where $M_{\max}$ denotes the highest order of the harmonics. According to Eq. (9), the cutoff energy depends on the maximum of the enhanced electric field $\Omega_{\max}$. We have shown in Fig. 2 that the maximum value of the enhanced electric field $\Omega_{\max}$ is sensitive to the field-strength ratio q and the relative phase ϕ. Thus one can control the cutoff energy by modulating q and ϕ.

To facilitate exploration of the underlying mechanism responsible for the cutoff extension modified by the field-strength ratio between the fundamental and the control fields, we first perform a classical simulation of the time profiles of field-dressed energies $\epsilon_\pm$. As shown in Figs. 3(a) and 3(b), the time evolution of adiabatic energies significantly depends on the field-strength ratio q. These results can be understood from the expression of $\epsilon_\pm$ that the adiabatic energies are effectively determined by $\Omega^2(t)$, whose maximal value of $\Omega(t)$ is sensitive to q. The larger energy difference corresponds to the higher harmonic generation at times t_2 where the avoided level crossings occur, and the maximal energy difference corresponds to the highest HHG at times t_{2M}. In the case of $\phi = 0$, we can obtain the positive root for different field-strength ratios q by solving Eq. (6) as

$$t_{2M} = \frac{2}{\omega_0}\arccos\left[\frac{1}{8}(-q \pm \sqrt{32 + q^2})\right]. \tag{10}$$

Equation (10) shows that the time t_{2M} yields different values for different field-strength ratios q. As illustrated in Figs. 3(a) and 3(b), the absolute maxima of adiabatic energies corresponding to the highest HHG occur, respectively, at $t_{2M} = 1.55T_0$ in the case of $q = 0.5$ and $t_{2M} = 1.60T_0$ in the case of $q = 0.8$. This is partially confirmed by Figs. 3(c) and 3(d), where the populations of the adiabatic states are plotted as functions of time (in units of the field cycle T_0). In Figs. 3(c) and 3(d), one can see that the avoided level crossings of the adiabatic states take place at time t_2, and the maximal avoided level crossings correspond to the times t_{2M}. In addition, there are several sharp peaks for both populations of the field-dressed state $|0\rangle^A$ and state $|1\rangle^A$ at times t_1, which indicates that most population transfer has taken place. However, there are several small peaks, which implies that population transfer also occurs at other times. Direct comparison of the cases $q = 0.5$ and $q = 0.8$ in Figs. 3(c) and 3(d) shows that the level crossings and avoided level crossings resulting from population transfer

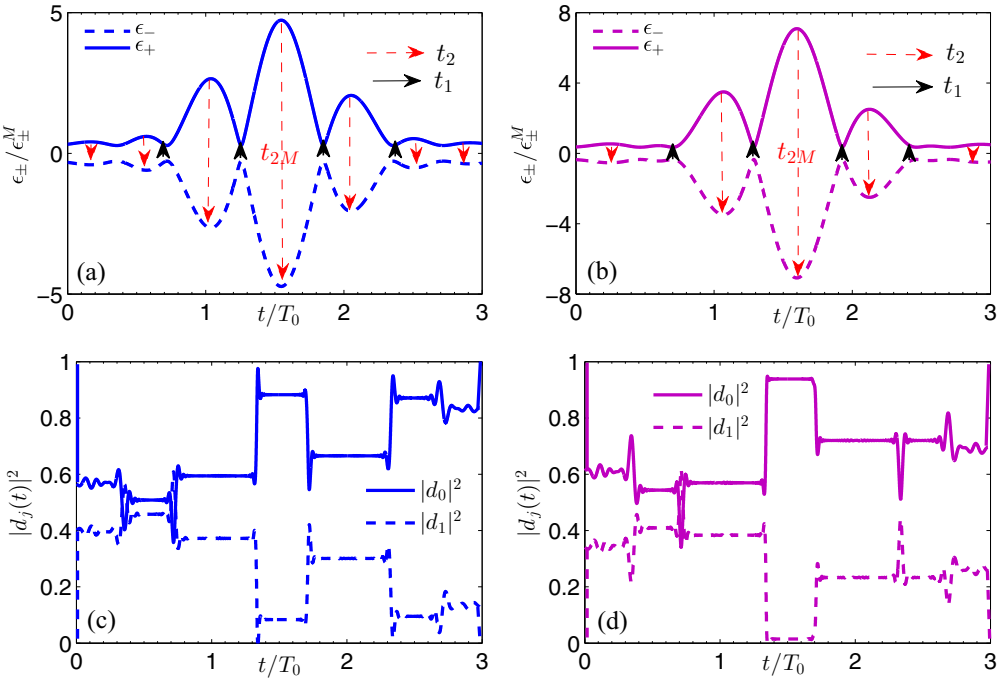

FIG. 3. (a),(b) Adiabatic energies (given in units of the maximal energy $\epsilon_\pm^M$) ϵ_+ (upward line) and ϵ_- (downward line) of the adiabatic states $|0\rangle^A$ and $|1\rangle^A$ for different cases, i.e., (a) $q = 0.5$ and (b) $q = 0.8$. (c),(d) Populations $|d_j(t)|^2$ of the corresponding adiabatic states, i.e., (c) $q = 0.5$ and (d) $q = 0.8$. Values of other parameters are chosen the same as in Fig. 2(a) except for $\phi = 0$.

between the adiabatic states have a sensitive dependence on the field-strength ratio q. The main reasons are based on the fact that near-field enhancement results from the MNP for a higher field-strength ratio induces a larger energy difference between the adiabatic states. In addition, Figs. 3(c) and 3(d) also show that the population transfers exhibit asymmetries very similar to the ones observed in the field-dressed energies. The broad level crossings of the adiabatic population evolution correspond to longer time intervals than the sharp level crossings, which causes the oscillations of $|d_j(t)|^2$ to exhibit asymmetric shapes. This asymmetry becomes pronounced slightly as the field-strength ratio q increases from 0.5 to 0.8.

Similar asymmetric features occur in the time evolution of the dipole acceleration $a(t)$. As shown in Figs. 4(a) and 4(b), the time evolution of $a(t)$ exhibits intense oscillations including nodes and antinodes, respectively, at the level-crossing times and avoided level-crossing times. In our previous work for only the fundamental driving case [43], the nodes corresponding to level-crossing times cover almost-equal temporal intervals. However, here for the bichromatic driving case, these equal temporal intervals are broken due to the application of the additional control pulse. Thus Figs. 4(a) and 4(b) exhibit narrower and broader nodes, corresponding to narrower and broader level-crossing times, respectively. Figures 4(c) and 4(d) show the modulus of the quantum time-frequency profile corresponding to the different field-strength ratios $q = 0.5$ and $q = 0.8$, respectively, obtained by the wavelet transform of the induced dipole acceleration in Eq. (5). One finds that the time-frequency spectra share a similar shape with the positive branch of the adiabatic energies in Figs. 3(a) and 3(b). These interesting results can be understood from Eq. (8), which indicates clearly that the harmonic order M is proportional to the adiabatic energy ϵ_+. For the case $q = 0.5$, there are three major emission bursts shown in Fig. 4(c). Similarly, for $q = 0.8$, there are three major emission bursts shown in Fig. 4(d). Each emission time remarkably corresponds to the avoided level-crossing times t_2. It should be noted that the center peak corresponding to the highest harmonic generation shown in Fig. 4(d) is considerably higher than that in Fig. 4(c). As a result, the maximum photon energy of the cutoff harmonics (corresponds to the center peaks) in Fig. 4(d) is extended by more than 120 harmonic orders compared with the one in Fig. 4(c). In addition, there is an obvious extension in the time-resolved spectra for the cutoff harmonics, with respect to the monochromatic case [43]. A plausible explanation regarding the cutoff extension mechanism is that due to the adiabatic energy's strong dependence on the field-strength ratio q, the time-frequency spectra of the dipole acceleration are q dependent as well.

Population transfer between the adiabatic states, and consequently the HHG spectra, can be modulated by the addition of a control field with a low frequency to the fundamental one. For direct insight into the influence of the field-strength ratio on the HHG process, we present the temporal profiles of harmonics near the cutoff region for two cases, (a) $q = 0.5$ and (b) $q = 0.8$ with fixed relative phase $\phi = 0$, by using the wavelet time-frequency analysis of the dipole acceleration in Fig. 5. The time profile of harmonics presented in Fig. 5(a) is from order $210\omega_0$ to order $250\omega_0$, and Fig. 5(b) is from order $310\omega_0$ to $390\omega_0$. In both cases, the time profiles exhibit steep peaks when the adiabatic energies reach their peak values, which contribute mainly to the HHG in the field. In addition,

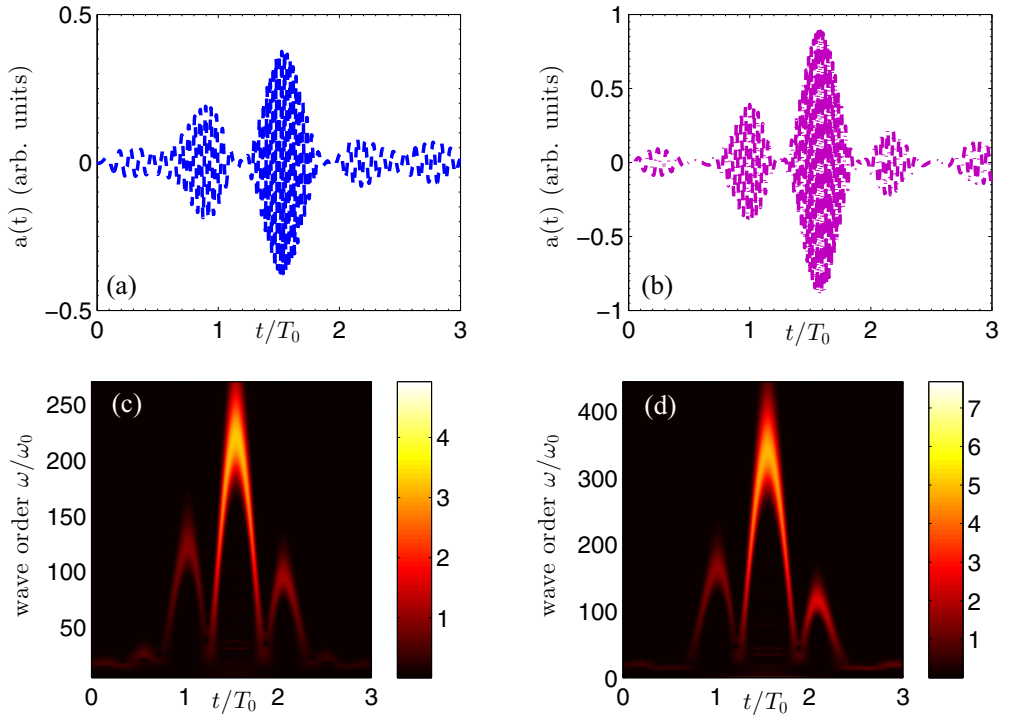

FIG. 4. (a),(b) Time evolution of dipole accelerations for different cases, i.e., (a) $q = 0.5$ and (b) $q = 0.8$. (c),(d) Wavelet time-frequency profiles of HHG power spectra of the Gaussian bichromatic pulse laser for (c) $q = 0.5$ and (d) $q = 0.8$. Values of other parameters are chosen the same as in Fig. 2(a) except for $\phi = 0$.

one finds that the peak intensity as well as the width of the harmonic profile becomes small as the order of harmonics increases. In addition, the main inner peak profile gradually gets wide and weak and splits into two peaks as the order of harmonics decreases. The physical interpretation of these features is rather clear. As the harmonics deviate from the cutoff energies and decrease, the avoided level crossings between two adiabatic states occur at two possible times (a shorter and a longer one) induced by quantum interference between two different paths, and thus two harmonic peaks occur. This picture is related to the level crossings and avoided level crossings induced by population transfers between adiabatic states.

As illustrated in Figs. 3–5, for a fixed relative phase $\phi = 0$, we have illustrated that the HHG spectra exhibit several well-formed individual peak structures in the cutoff region, which correspond to single-peak harmonic shapes and can, in principle, be controlled to produce a stronger radiation emission via modulation of the field-strength ratio q. The main contribution to the highest harmonic generation is the maximal energy difference $\epsilon_+ - \epsilon_-$, which is dependent on the field-strength ratio. We have shown in Fig. 2 that the spectra of the enhanced field and the HHG can also be modulated by the relative phase ϕ between the fundamental field and the low-frequency control field. For $\phi = \pi/2$, Eqs. (6) and (7) imply that there exist different values of avoided level-crossing times t_{2M} and level-crossing times t_1 as in the case of $\phi = 0$. In order to facilitate exploration of the underlying mechanism responsible for the HHG modified by the relative phase ϕ, we present in Fig. 6(a) the adiabatic states as functions of time with

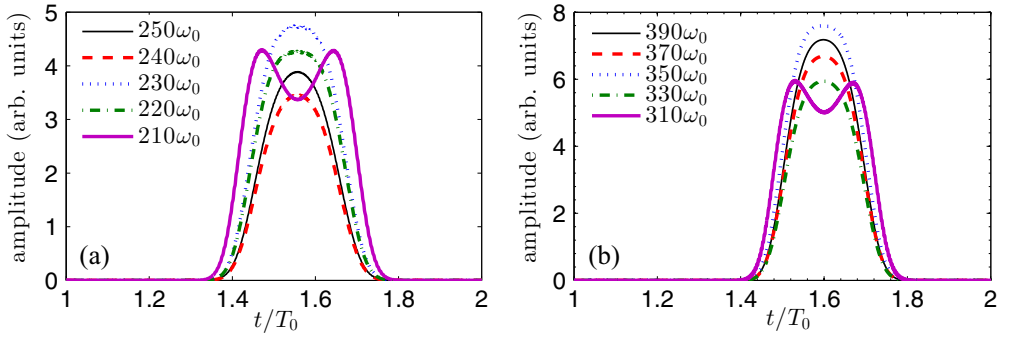

FIG. 5. Time profiles of harmonics with different frequencies for the cases (a) $q = 0.5$ and (b)$q = 0.8$. The different harmonic frequencies are shown. Other parameters are the same as in Fig. 4.

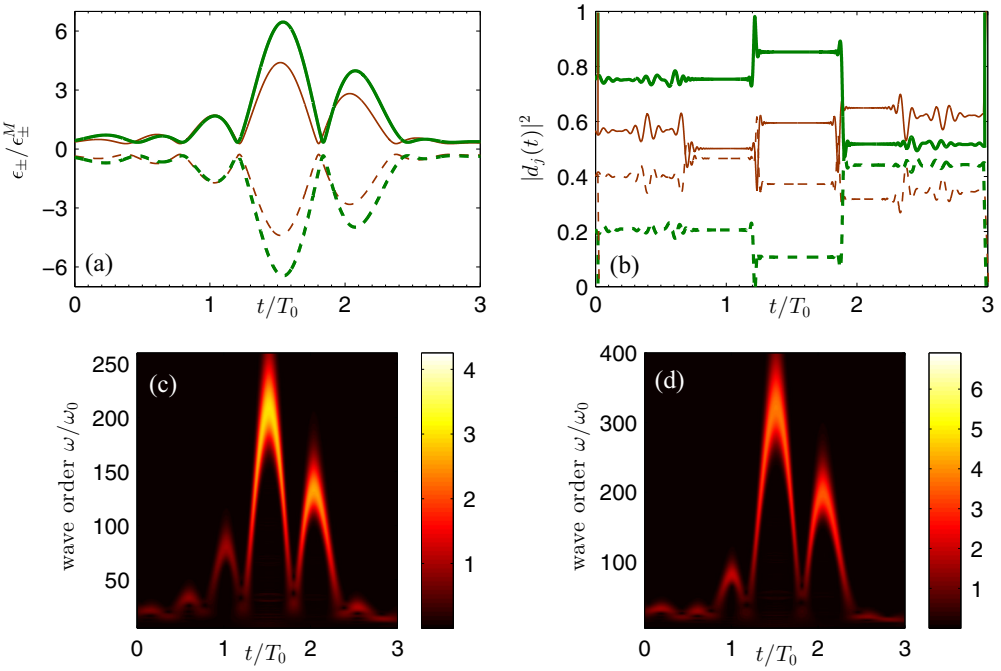

FIG. 6. (a) Adiabatic energies (given in units of the maximal energy $\epsilon_\pm^M$) ϵ_+ (upward line) and ϵ_- (downward line) of the adiabatic states $|0\rangle^A$ and $|1\rangle^A$, where thin and thick lines correspond to $q = 0.5$ and $q = 0.8$, respectively. (b) Populations $|d_0(t)|^2$ (upward line) and $|d_1(t)|^2$ (downward line) of the corresponding adiabatic states with respect to (a). (c),(d) Wavelet time-frequency profiles of HHG power spectra of the Gaussian bichromatic pulse laser for (c) $q = 0.5$ and (d) $q = 0.8$, respectively. Values of other parameters are chosen the same as in Fig. 3 except for $\phi = \pi/2$.

$\phi = \pi/2$, for $q = 0.5$ (thin lines) and $q = 0.8$ (thick lines). The comparison between the results for $\phi = 0$ and $\phi = \pi/2$ shows that level crossings and avoided level crossings, as well as the maximal adiabatic energies, show a tiny dependence on the relative phase ϕ. Compared with the results for $\phi = 0$, one finds that the avoided level-crossing times corresponding to the maximal energies shift slightly in the case of $\phi = \pi/2$, i.e., $t_{2M} \approx 1.54T_0$ for $q = 0.5$ and $t_{2M} \approx 1.58T_0$ for $q = 0.8$, which can be directly confirmed by Eq. (6). In addition, this figure shows that the maximal adiabatic energies for $\phi = \pi/2$ are slightly lower than the ones for $\phi = 0$. In order to examine how the changes in the adiabatic-state energies induced by varying relative phases ϕ modify the HHG process, as in the previous discussion for $\phi = 0$, we present the analysis of the time-dependent adiabatic-state population and time-frequency spectra for $\phi = \pi/2$. As shown in Fig. 6(b), the changes in the avoided level crossings at t_{2M} predicted by Eq. (6) yield to the shifts in the maximal adiabatic energies. We now investigate the cutoff and plateau harmonics, obtained from the wavelet transform of the induced dipole acceleration in Eq. (5), for different field-strength ratios q with $\phi = \pi/2$. In comparison to the situation where $\phi = 0$, Figs. 6(c) and 6(d) show that the main peaks for the highest harmonics are slightly lower than the ones shown in Figs. 4(c) and 4(d). In other words, the maximal adiabatic energies, and consequently the HHG spectra, are insensitive to the relative phase between the fundamental and the additional low-frequency control pulses.

Interestingly enough, the plasmonic enhanced field spectra and adiabatic energies, and consequently the HHG process, will exhibit completely different situations when the bichromatic field is synthesized by a fundamental pulse and an additional high-frequency control pulse. Without any loss of generality, we use the following bichromatic pulse with the electric field:

$$E(t) = E_0 f(t) \sin[\omega_0(t - 2T_0)] + q E_0 f(t) \sin[2\omega_0(t - 2T_0) + \phi]. \quad (11)$$

As an example, at a fixed field-strength ratio $q = 0.5$, we study the plasmonic field enhancement and time evolution of the adiabatic energies, as well as the HHG spectra, for $\phi = 0$ and $\phi = \pi/2$. The corresponding plasmonic field enhancement spectra of the MNP for different relative phases (i.e., $\phi = 0$ and $\phi = \pi/2$) are shown in Fig. 7(a). Differently from the results for the case with an additional low-frequency pulse in the spectra shown in Fig. 2(a), the relative phase obviously plays an important role in plasmonic field enhancement in the case of an additional high-frequency control pulse. Furthermore, the field-dependent adiabatic energies, as well as the level-crossing times and avoided level-crossing times, also depend significantly on the relative phase. As illustrated in Fig. 7(b), a relatively weak high-frequency wave considerable distorts the level crossings and, consequently, the maxima of the adiabatic energies in the case of $\phi = \pi/2$. In order to examine how the distortions of the adiabatic energies resulting from varying relative phases ϕ modify the HHG process, we present a time-frequency analysis of the HHG spectra, as shown in Figs. 7(c) and 7(d). In comparison to the case of $\phi = 0$, one finds that the spectral peak splits and occurs at

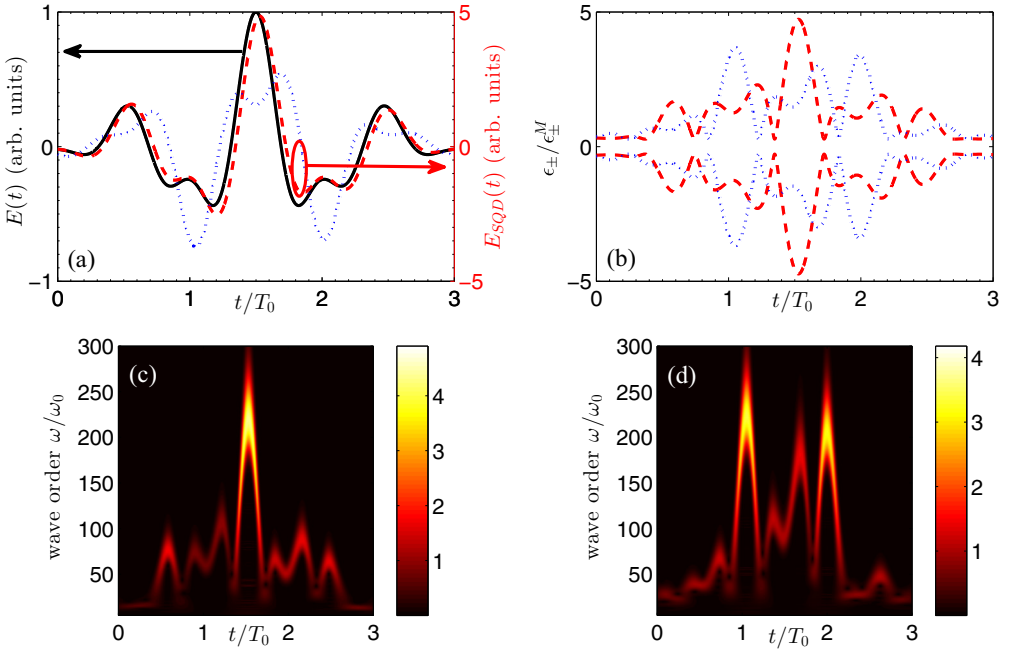

FIG. 7. (a) Field enhancement of an MNP on an incident Gaussian-shaped bichromatic pulse for different relative phases ϕ, i.e., $\phi = 0$ (dashed line) and $\phi = \pi/2$ (dotted line). (b) Adiabatic energies (given in units of the maximal energy $\epsilon_{\pm}^{M}$) ϵ_{+} (upward line) and ϵ_{-} (downward line) of the adiabatic states $|0\rangle^{A}$ and $|1\rangle^{A}$, i.e., $\phi = 0$ (dashed line) and $\phi = \pi/2$ (dotted line). (c),(d) Wavelet time-frequency profiles of HHG power spectra of the Gaussian bichromatic pulse laser for (c) $\phi = 0$ and (d) $\phi = \pi/2$, respectively. Values of other parameters are chosen the same as in Fig. 3 except for $q = 0.5$.

two times, $t_{2M} \approx T_0$ and $2T_0$ for $\phi = \pi/2$, which agrees with the prediction in Ref. [16]. These phenomena are intuitively traceable in the splitting of the maximal values of the adiabatic energies in the case of $\phi = \pi/2$.

As illustrated in Fig. 2(b), we find that the harmonic spectra exhibit several well-formed individual peak structures near the cutoff region for $\phi = 0$, which corresponds to the single-peak harmonic shapes and can, in principle, be superimposed on each other to produce a stronger radiation emission. As an example, we show in Fig. 8(a) the harmonic spectra with a fixed relative phase $\phi = 0$ for different field-strength ratios q, i.e., $q = 0.5$ (solid line) and $q = 0.8$ (dashed line). One can clearly see that a smooth supercontinuum is generated though the plateau to the cutoff for both cases, $q = 0.5$ and $q = 0.8$, which implies that an ultrashort XUV pulse is available. In Fig. 8(b), we present the temporal profiles of the corresponding ultrashort XUV pulses. The ultrashort XUV pulses are obtained by synthesizing the supercontinuum from $140\omega_0$ to $230\omega_0$ and from $250\omega_0$ to $340\omega_0$ for the cases of $q = 0.5$ and $q = 0.8$, respectively. As shown in Fig. 8(b), single ultrashort XUV pulses are obtained in both cases. The durations of the pulses corresponding to these two cases are about 2.98 and 2.48 fs, respectively. Moreover, this figure also shows that the intensity of the isolated ultrashort XUV pulses increases as the field-strength ratio q increases, which is related to the population transfers and acceleration properties in the few-cycle bichromatic field. Such isolated ultrashort XUV pulses are beneficial for detecting and controlling the

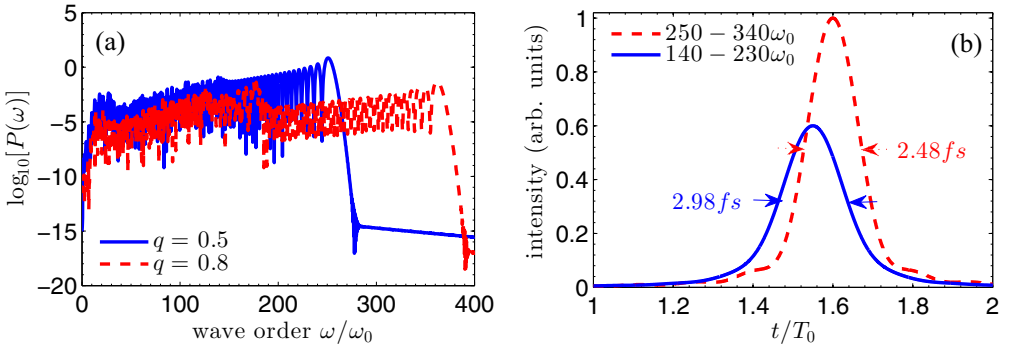

FIG. 8. (a) Harmonic spectra in a bichromatic field with fixed relative phase $\phi = 0$ for different field-strength ratios q. (b) Temporal profiles of the generated isolated ultrashort XUV pulses obtained by synthesizing the supercontinuum shown in (a). Other parameters are the same as in Fig. 3.

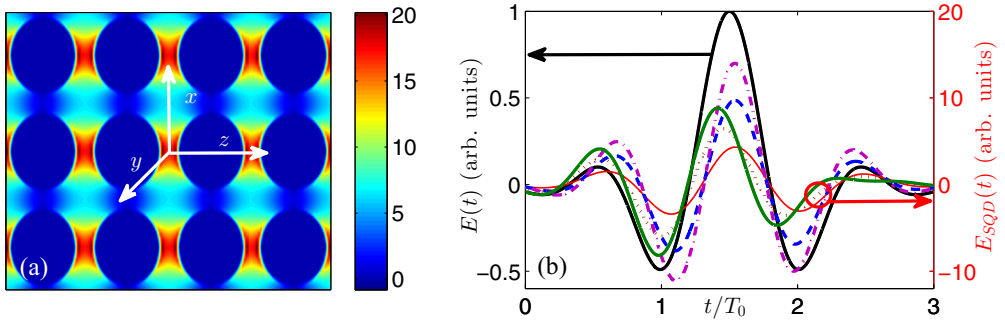

FIG. 9. (a) Contour plot of the enhanced fields between MNPs obtained by considering the ordered MNP array with a radius of $a = 7.5$ nm and a gap between MNPs of 4 nm (the centers between two MNPs are separated by a distance of 19 nm). The SQD is above the center of the gap along the y axis on the x-z plane and the distance between the SQD and the center of the adjacent MNP is $R = 11$ nm. The incident bichromatic few-cycle pulse propagates along the y axis with polarization along the z axis. (b) Field enhancement of MNP on the incident Gaussian-shaped bichromatic pulse for different field-strength ratios q and relative phases ϕ, i.e., $q = 0$ (solid line); $q = 0.5$, $\phi = 0$ (dashed line); $q = 0.5$, $\phi = \pi/2$ (dotted line); $q = 0.8$, $\phi = 0$ (dash-dotted line); and $q = 0.8$, $\phi = \pi/2$ (thick solid line). Other parameters are the same as in Fig. 2.

ultrafast dynamics induced by the electric field rather than the intensity profile. Besides, the bichromatic plasmonic near fields for single ultrashort XUV pulse generation, which are generated when an MNP is subjected to a moderate-intensity ($< 10^{12}$ W/cm^2) bichromatic few-cycle pulse, is more easily available than the complex and expensive femtosecond laser amplifier systems.

As the main contribution to the highest harmonic generation is the maximal energy difference between the adiabatic states $|0\rangle^A$ and $|1\rangle^A$, we have shown that a plasmonic enhanced bichromatic field in an MNP can be used to enhance the adiabatic energies and, consequently, modify the HHG process via variation of the field-strength ratio and the relative phase between the fundamental and the control pulses. Instead of a single MNP, for a more realistic case, we should study HHG utilizing plasmonic enhanced fields in an ordered array of MNPs. In the ordered array of gold MNPs, each spherical MNP has radius $a = 7.5$ nm and the center-to-center distance between two MNPs is 19 nm (i.e., the gap size is 4 nm). In our simulation, the bichromatic few-cycle pulse is synthesized by a fundamental pulse and a control pulse with the same electric field from Eq. (1). The incident bichromatic few-cycle pulse propagates along the y axis with polarization along the z axis. The contour plot of the enhanced fields between the MNPs considering this ordered MNP array is shown in Fig. 9(a). In this figure, one can see that the maximal enhancement of the field is located in the gap of the x-z plane, and the enhancement of the field is lower along the y axis. We consider that the SQD is along the y axis and located above the center of the gap in the x-z plane, with the distance between the SQD and the center of the adjacent MNP $R = 11$ nm. The corresponding plasmonic field enhancement spectra of the MNP for different field-strength ratios (i.e., $q = 0, q = 0.5$, and $q = 0.8$) and different relative phases (i.e., $\phi = 0$ and $\phi = \pi/2$) are shown in Fig. 9(b). We may compare the field enhancement factor of the MNP array with that of a single MNP shown in Fig. 2(a). The maximal field enhancement exceeds 15 for $q = 0.8$ and $\phi = 0$ at the location of the SQD and is higher towards the x-z plane. In addition, Fig. 9(b) also shows that the field-strength ratio and relative phase have an influence on the field enhancement similar to that of the single MNP case shown Fig. 2(a). The field enhancement factor increases as the field-strength ratio increases from 0.5 to 0.8 and the location of the center peaks of the enhanced fields shifts slightly as the relative phase changes from 0 to $\pi/2$. Since the maximal field enhancement exceeds 15 in an ordered array of MNPs and is much higher than the maximal enhancement in the single-MNP case, one can expect that the cutoff energies of HHG can be extended in comparison to the case with a single MNP.

IV. CONCLUSION

In conclusion, we have theoretically investigated high-order-harmonic generation in a semiconductor quantum dot and metallic nanoparticle complex driven by a moderate-intensity ($<10^{12}$ W/cm^2) bichromatic few-cycle pulse. Bichromatic plasmonic near fields, which depend on temporal waveform synthesis, are generated. Our numerical results illustrate that modulating the field-strength ratio and modulating the relative phase between the fundamental and the control fields are efficient methods for controlling HHG spectra and are capable of generating broader supercontinuum XUV pulse harmonics with higher cutoff orders. Differently from our previous work [43], where HHG spectra were controlled via modulation of the interparticle distance between the SQD and the MNP, here these new degrees of freedom (the field-strength ratio and relative phase) could lead to an enhancement in the harmonic spectra to the XUV regime. By using the two-level atom as a simplified model, HHG modified by the field-strength ratio and relative phase can be successfully explained in adiabatic-state transition. Furthermore, we conducted the time-frequency analysis by using the wavelet transform of the induced dipole acceleration and found that the time-frequency spectra are proportional to the energies of the adiabatic states. As a matter a fact, this feature is a consequence of the enhanced bichromatic plasmonic near fields, which substantially modify the adiabatic-state transition via the field-strength ratio and relative phase. More interestingly, by choosing a suitable time profile of the incident bichromatic pulse, the temporal harmonic profile can be superimposed,

i.e., ultrabroad supercontinuum harmonic spectra will be generated and isolated ultrashort XUV pulses can be obtained. In addition, the plasmonic field enhancement in a realistic ordered array of gold nanoparticles is discussed qualitatively. In this case, the maximal field enhancement exceeds 15 in an ordered array of MNPs, and thus one can expect that the cutoff energies of HHG can be extended in comparison to the case with a single MNP.

ACKNOWLEDGMENTS

We appreciate useful discussions with Y. Wu. This research was supported in part by the National Natural Science Foundation of China under Grants No. 11374050 and No. 61372102, by the Qing Lan project of Jiangsu, and by Fundamental Research Funds for the Central Universities under Grant No. 2242012R30011.

[1] A. McPherson, G. Gibson, H. Jara, U. Johann, T. S. Luk, I. A. McIntyre, K. Boyer, and C. K. Rhodes, J. Opt. Soc. Am. B **4**, 595 (1987).

[2] A. L'Huillier, K. J. Schafer, and K. C. Kulander, J. Phys. B **24**, 3315 (1991).

[3] T. Brabec and F. Krausz, Rev. Mod. Phys. **72**, 545 (2000).

[4] P. B. Corkum, Phys. Rev. Lett. **71**, 1994 (1993).

[5] M. Lewenstein, P. Balcou, M. Y. Ivanov, A. L'Huillier, and P. B. Corkum, Phys. Rev. A **49**, 2117 (1994).

[6] K. J. Schafer, B. Yang, L. F. DiMauro, and K. C. Kulander, Phys. Rev. Lett. **70**, 1599 (1993).

[7] F. Krausz and M. Ivanov, Rev. Mod. Phys. **81**, 163 (2009).

[8] G. Sansone, L. Poletto, and M. Nisoli, Nat. Photon. **5**, 655 (2011).

[9] M. Schultze, M. Fiess, N. Karpowicz, J. Gagnon, M. Korbman, M. Hofstetter, S. Neppl, A. L. Cavalieri, Y. Komninos, Th. Mercouris, C. A. Nicolaides, R. Pazourek, S. Nagele, J. Feist, J. Burgdörfer, A. M. Azzeer, R. Ernstorfer, R. Kienberger, U. Kleineberg, E. Goulielmakis, F. Krausz, and V. S. Yakovlev, Science **328**, 1658 (2010).

[10] G. Sansone, F. Kelkensberg, J. F. Pérez-Torres, F. Morales, M. F. Kling, W. Siu, O. Ghafur, P. Johnsson, M. Swoboda, E. Benedetti, F. Ferrari, F. Lépine, J. L. Sanz-Vicario, S. Zherebtsov, I. Znakovskaya, A. L'huillier, M. Y. Ivanov, M. Nisoli, F. Martin, and M. J. J. Vrakking, Nature **465**, 763 (2010).

[11] M. I. Stockman, M. F. Kling, U. Kleineberg, and F. Krausz, Nat. Photon. **1**, 539 (2007).

[12] A. L. Cavalieri, N. Müller, Th. Uphues, V. S. Yakovlev, A. Baltuška, B. Horvath, B. Schmidt, L. Blümel, R. Holzwarth, S. Hendel, M. Drescher, U. Kleineberg, P. M. Echenique, R. Kienberger, F. Krausz, and U. Heinzmann, Nature **449**, 1029 (2007).

[13] M. Lenzner, J. Krüger, S. Sartania, Z. Cheng, Ch. Spielmann, G. Mourou, W. Kautek, and F. Krausz, Phys. Rev. Lett. **80**, 4076 (1998).

[14] O. E. Alon, V. Averbukh, and N. Moiseyev, Phys. Rev. Lett. **80**, 3743 (1998).

[15] F. I. Gauthey, B. M. Garraway, and P. L. Knight, Phys. Rev. A **56**, 3093 (1997).

[16] C. Figueira de Morisson Faria and I. Rotter, Phys. Rev. A **66**, 013402 (2002).

[17] J. C. A. Barata and W. F. Wreszinski, Phys. Rev. Lett. **84**, 2112 (2000).

[18] Y. Wu and X. Yang, Phys. Rev. Lett. **98**, 013601 (2007).

[19] P. Huang, X.-T. Xie, X. Lü, J. Li, and X. Yang, Phys. Rev. A **79**, 043806 (2009).

[20] J. Wu, H. Qi, and H. Zeng, Phys. Rev. A **77**, 053412 (2008).

[21] Y. Wu and X. Yang, Phys. Rev. A **76**, 013832 (2007).

[22] S. Kim, J. Jin, Y.-J. Kim, I.-Y. Park, Y. Kim, and S.-W. Kim, Nature **453**, 757 (2008).

[23] J. Choi, S. Kim, I. Y. Park, D. H. Lee, S. Han, and S. W. Kim, New J. Phys. **14**, 103038 (2012).

[24] A. Husakou, F. Kelkensberg, J. Herrmann, and M. J. J. Vrakking, Opt. Express **19**, 25346 (2011).

[25] A. Husakou, S. J. Im, and J. Herrmann, Phys. Rev. A **83**, 043839 (2011).

[26] S. L. Stebbings, F. Sémann, Y. Y. Yang, A. Scrinzi, M. Durach, A. Rusina, M. I. Stockman, and M. F. Kling, New J. Phys. **13**, 073010 (2011).

[27] M. Sivis, M. Duwe, B. Abel, and C. Ropers, Nature **485**, E1 (2012).

[28] S. Kim, J. Jin, Y.-J. Kim, I.-Y. Park, Y. Kim, and S.-W. Kim, Nature **485**, E1 (2012).

[29] S. Zherebtsov, T. Fennel, J. Plenge, E. Antonsson, I. Znakovskaya, A. Wirth, O. Herrwerth, F. Süßmann, C. Peltz, I. Ahmad, S. A. Trushin, V. Pervak, S. Karsch, M. J. J. Vrakking, B. Langer, C. Graf, M. I. Stockman, F. Krausz, E. Rühl, and M. F. Kling, Nat. Phys. **7**, 656 (2011).

[30] F. Süßmann and M. F. Kling, Phys. Rev. B **84**, 121406(R) (2011).

[31] Y.-Y. Yang, A. Scrinzi, A. Husakou, Q.-G. Li, S. L. Stebbings, F. Süßmann, H.-J. Yu, S. Kim, E. Rühl, J. Herrmann, X. C. Lin, and M. F. Kling, Opt. Express **21**, 2195 (2013).

[32] G. Herink, D. R. Solli, M. Gulde, and C. Ropers, Nature **483**, 190 (2012).

[33] P. Hommelhoff, Y. Sortais, A. Aghajani-Talesh, and M. A. Kasevich, Phys. Rev. Lett. **96**, 077401 (2006).

[34] M. Schenk, M. Krüger, and P. Hommelhoff, Phys. Rev. Lett. **105**, 257601 (2010).

[35] M. Krüger, M. Schenk, and P. Hommelhoff, Nature **475**, 78 (2011).

[36] M. Krüger, M. Schenk, M. Förster, and P. Hommelhoff, J. Phys. B **45**, 074006 (2012).

[37] I.-Y. Park, S. Kim, J. Choi, D.-H. Lee, Y.-J. Kim, M. F. Kling, M. I. Stockman, and S.-W. Kim, Nat. Photon. **5**, 677 (2011).

[38] I.-Y. Park, J. Choi, D.-H. Lee, S. Han, S. Kim, and S.-W. Kim, Ann. Phys. (Berlin) **525**, 87 (2013).

[39] J. A. Péréz-Hernandez, M. F. Ciappina, M. Lewenstein, L. Roso, and A. Zaïr, Phys. Rev. Lett. **110**, 053001 (2013).

[40] T. Shaaran, M. F. Ciappina, R. Guichard, J. A. Péréz-Hernandez, L. Roso, M. Arnold, T. Siegel, A. Zaïr, and M. Lewenstein, Phys. Rev. A **87**, 041402(R) (2013).

[41] B. Fetic and D. B. Milosevic, J. Mod. Opt. **60**, 1466 (2013).

[42] B. Fetic, K. Kalajdzic, and D. B. Milosevic, Ann. Phys. **525**, 107 (2013).

[43] Z. W. Huang, A. X. Chen, Z. Zhang, and W. X. Yang, Europhys. Lett. **111**, 24005 (2015).

[44] W. X. Yang, Opt. Lett. **40**, 4903 (2015).
[45] W. Zhang, A. O. Govorov, and G. W. Bryant, Phys. Rev. Lett. **97**, 146804 (2006).
[46] M. T. Cheng, S. D. Liu, H. J. Zhou, Z. H. Hao, and Q. Q. Wang, Opt. Lett. **32**, 2125 (2007).
[47] J. Y. Yan, W. Zhang, S. Q. Duan, X. G. Zhao, and A. O. Govorov, Phys. Rev. B **77**, 165301 (2008).
[48] S. L. Sewall, A. Franceschetti, R. R. Cooney, A. Zunger, and P. Kambhampati, Phys. Rev. B **80**, 081310(R) (2009).
[49] P. Antoine, B. Piraux, and A. Maquet, Phys. Rev. A **51**, R1750 (1995).
[50] X. M. Tong and Shih-I. Chu, Phys. Rev. A **61**, 021802(R) (2000).
[51] S. M. Sadeghi and R. G. West, J. Phys.: Condens. Matter **23**, 425302 (2011).
[52] R. D. Artuso and G. W. Bryant, Phys. Rev. B **82**, 195419 (2010).
[53] E. Paspalakis, S. Evangelou, and A. F. Terzis, Phys. Rev. B **87**, 235302 (2013).
[54] P. B. Johnson and R. W. Christy, Phys. Rev. B **6**, 4370 (1972).
[55] H. Xiong, L. G. Si, X. Y. Lu, X. Yang, and Y. Wu, Opt. Lett. **38**, 353 (2013).